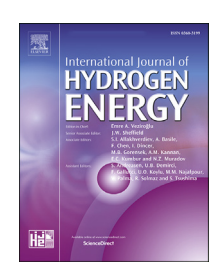


Available online at www.sciencedirect.com

# **ScienceDirect**





# Preparation of CdS-CoS<sub>x</sub> photocatalysts and their photocatalytic and photoelectrochemical characteristics for hydrogen production



Lizi Chu <sup>a,1</sup>, Yuan Lin <sup>a,1</sup>, Yunpeng Liu <sup>a</sup>, Hongjuan Wang <sup>a</sup>, Qiao Zhang <sup>b</sup>, Yuhang Li <sup>b</sup>, Yonghai Cao <sup>a</sup>, Hao Yu <sup>a</sup>, Feng Peng <sup>b,\*</sup>

- <sup>a</sup> School of Chemistry and Chemical Engineering, Key Laboratory of Fuel Cell Technology of Guangdong Province, South China University of Technology, Guangzhou, 510640, China
- <sup>b</sup> Guangzhou Key Laboratory for New Energy and Green Catalysis, School of Chemistry and Chemical Engineering, Guangzhou University, Guangzhou, 510006, China

#### HIGHLIGHTS

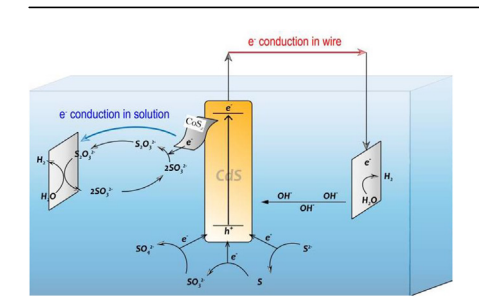
- CoS<sub>x</sub> as co-catalyst is loaded on CdS nanorod by a facile method.
- CdS-CoS<sub>x</sub> has good activity and stability for photoelectrochemical (PEC) reaction.
- PEC activity of CdS-CoS<sub>x</sub> as photoanode for H<sub>2</sub> production is the same as that of CdS-Pt.
- An abnormal relationship between photocurrent and hydrogen production is found.
- The reaction network in Na<sub>2</sub>S
   -Na<sub>2</sub>SO<sub>3</sub> system for PEC H<sub>2</sub> production is proposed.

## ARTICLE INFO

Article history:
Received 26 June 2019
Received in revised form
30 August 2019
Accepted 4 September 2019
Available online 30 September 2019

Keywords: Photocatalyst Photocatalysis

#### GRAPHICAL ABSTRACT



## ABSTRACT

A facile method of loading  $CoS_x$  nanosheet onto CdS nanorod has been designed, and the prepared CdS- $CoS_x$  composite catalyst exhibited significantly improved performance for photocatalytic hydrogen evolution compared with CdS catalyst. This composite catalyst was also used as a photoanode for photoelectrochemical (PEC) hydrogen production. The hydrogen production rate reached 168.6  $\mu$ mol cm $^{-2}$  h $^{-1}$  (37.77 L m $^{-2}$  h $^{-1}$ ) under the simulated solar light, which is 2.7 times that of CdS and the same as that of CdS–Pt. In addition, in the Na<sub>2</sub>S–Na<sub>2</sub>SO<sub>3</sub> system for PEC hydrogen production, an abnormal relationship between photocurrent and the hydrogen production yield was found. By designing a series of experiments, the photocatalytic and photoelectrochemical characteristics for hydrogen production were reasonably revealed for the first time. In this work, the prepared

<sup>\*</sup> Corresponding author.

E-mail address: fpeng@gzhu.edu.cn (F. Peng).

<sup>&</sup>lt;sup>1</sup> These authors contribute equally.

Photoelectrochemical hydrogen production Cobalt sulfide Cadmium sulfide structured catalyst is easy to be recycled, and  $CoS_x$  can replace precious metal Pt, showing a promising application.

© 2019 Hydrogen Energy Publications LLC. Published by Elsevier Ltd. All rights reserved.

#### Introduction

Due to the exhaustion of non-renewable resources such as fossil fuels and increasingly serious environmental pollution, the search for clean and non-polluting sustainable energy has attracted extensive interest of researchers around the world. Hydrogen is an excellent energy carrier due to its advantages of high energy density and environmental friendliness. Photocatalytic water-splitting is a promising way to produce hydrogen. However, there is a long way to go for its large-scale application for hydrogen production because of the relatively low energy conversion efficiency of photocatalysis at present. Therefore, it is still a challenge to find a photocatalytic material with high utilization efficiency of sunlight and good stability [1—11].

Among many photocatalytic materials, metallic sulfides have been widely studied due to their narrow band gaps and high utilization of solar light. CdS with the band gap of 2.4eV, as a typical semiconductor photocatalytic material, has good response to visible light and high conduction band position, which is favorable to reduce H<sup>+</sup> to hydrogen. Therefore, it has become a research hotspot [12-18]. However, CdS is easily oxidized by photogenerated holes, resulting in self-corrosion. Moreover, CdS has high photogenerated carrier recombination rate, which leads to its poor photocatalytic performance for hydrogen production [19-21]. Therefore, loading co-catalysts or combining other semiconductors to form heterostructures are effective ways to improve the photocatalytic activity and stability for hydrogen production [22-27]. It is well known that Pt and other precious metals are excellent co-catalysts for hydrogen evolution, but the high price and scarce resource make them unsuitable to be applied in a large scale [28-30]. Therefore, it is highly necessary to look for cheap and abundant non-precious metal catalysts to replace Pt and other precious metals as co-catalysts of CdS for photocatalytic hydrogen production [31-38].

Recently, non-noble metal sulfide has become a research hotspot of co-catalyst, such as  $Co_9S_8$ , which is a very promising catalytic material for photocatalytic hydrogen production because of narrow band gap and high flat band potential [39–42].  $CoS_x$  is widely used in electrocatalytic water decomposition and oxygen reduction with excellent electrochemical properties [43,44]. However, as far as we know,  $CoS_x$  has not been widely used in photocatalytic water-splitting. Qiu et al. [40] designed and synthesized a kind of direct Z-type semiconductor heterostructure photocatalytic material  $Co_9S_8/CdS$  with hollow  $Co_9S_8$  nano-cube supported CdS quantum dots. In this study, hollow cube  $Co(OH)_2$  was used as a template, and dimethyl sulfoxide (DMSO) was used as a solvent and S source to form  $Co_9S_8$  by

ion exchange with OH-. In visible light, compared with the pure hollow Co<sub>9</sub>S<sub>8</sub> cube and CdS quantum dot, the hydrogen production yield of the Co<sub>9</sub>S<sub>8</sub>/CdS catalyst was improved by 134 times and 9.1 times, respectively. In addition, the hydrogen production activity of the Co<sub>9</sub>S<sub>8</sub>/CdS catalyst remained relatively stable for 25 h. However, this method required the use of toxic organic reagents and complex preparation processes. Reddy [45] designed and synthesized a Z-type photocatalyst composed of Co-C@Co<sub>9</sub>S<sub>8</sub> doubleshell nanocage supported mesoporous reticular hydrogen production 26.69 mmol  $g^{-1} h^{-1}$  and an apparent quantum yield of 7.82% at 425 nm for 5 h. Wang et al. synthesized a photocatalyst with layered Co<sub>9</sub>S<sub>8</sub>@ZnIn<sub>2</sub>S<sub>4</sub> cage heterostructure [46], which effectively promoted the separation of photogenerated charges and exposed the redox active sites. The hydrogen production efficiency reached 6.25 mmol g<sup>-1</sup> h<sup>-1</sup> with good stability, but the disadvantage was that the powder sample was difficult to be recycled. Zheng et al. [41] designed and synthesized a CoS bifunctional catalyst with the hydrogen production rate of 1.197 mmol g<sup>-1</sup> h<sup>-1</sup>, and the oxygen yield of up to 65%. Lin's research group [47] used Co<sub>9</sub>S<sub>8</sub> for the first time to prepare a ternary TiO2/Co3S8/POM composite material as photoanode for photoelectrochemical (PEC) water oxidation, and the current density was as high as 1.12 mA cm<sup>-2</sup> vs RHE at AM1.5. However, the preparation process of this material was too complicated.

Here, a simple method was designed to synthesize a composite catalyst by using CdS nanorod array (NRs) as skeleton, and then loading CoS<sub>x</sub> nanosheet onto the CdS nanorod. According to the previous work of our research group [48], firstly, one-dimensional CdS NRs were grown on FTO, and then the intermediate containing Co was loaded onto the CdS NRs through simple chemical bath deposition (CBD) [49] in cobalt chloride and urea solution. Finally, CdS-CoSx was obtained through simple ion exchange. The preparation process is simple and the prepared structured catalyst is easy to be recycled. The photocatalytic hydrogen evolution performance of CdS-CoSx composite catalyst was significantly improved compared with that of single component catalyst CdS. The prepared composite catalyst was used as a photoanode for PEC hydrogen production, and its performance was comparable to that of CdS-Pt sample. So CoS<sub>x</sub> can replace precious metal Pt, showing a promising application. In addition, in Na<sub>2</sub>S-Na<sub>2</sub>SO<sub>3</sub> system for PEC hydrogen production, we found that the measured photocurrent showed an opposite change rule with the hydrogen production yield. By designing a series of experiments, the reaction network for this photocatalytic system was analyzed for the first time, and the photocatalytic and photoelectrochemical hydrogen production process was explained reasonably.

## **Experimental**

#### Catalysts preparation

One-dimensional CdS NRs were synthesized according to the hydrothermal methods reported previously by our group [48]. In a typical experiment, a clean 3  $\times$  5 cm² FTO with the conductive side facing down was immersed in Teflon-lined stainless steel autoclave (100 mL) containing 0.05 mol/L cadmium nitrate (99% Aladdin), 0.05 mol/L thiourea (99% Aladdin) and 0.01 mol/L glutathione (99% Aladdin), and then the autoclave was transferred to an oven and maintained at 210 °C for 12 h. After that, the CdS NRs film on FTO was alternately rinsed with distilled water and alcohol for several times, dried naturally, then annealed at 450 °C for 2 h under pure Ar.

The obtained CdS NRs film on FTO (conductive side facing down) was immersed in mixed solution containing 0.01 mol/L urea (99% Aladdin) and 0.015 mol/L cobalt chloride (99% Aladdin) under 90 °C for 1 h, 2 h, 3 h, 4 h, respectively, to load the intermediate containing cobalt (Co(CO<sub>3</sub>)0.35Cl<sub>0.20</sub>(OH)<sub>1.10</sub>, LCCH) [49] onto the CdS nanorods. After cooling down, the asprepared samples were transferred to Teflon-lined stainless-steel autoclaves (100 mL) containing 5 mmol/L Na<sub>2</sub>S solution. Then the autoclave was maintained at 90 °C for 21 h. Finally, the sample was rinsed, dried, and the resultant sample was labeled as CdS-CoS<sub>x</sub>-t, where "t" represented the chemical deposition time (1–4 h). The catalyst preparation process is illustrated in Scheme 1.

For comparison, CdS–Pt catalyst was prepared using the currently accepted photochemical reduction method. 300  $\mu L$  0.01 mol/L of  $H_2PtCl_6$  and 300  $\mu L$  of absolute ethanol were uniformly mixed, dropped on the CdS nanorods prepared above. The sample was then in situ photo-deposited under AM 1.5. The obtained sample was labeled as CdS–Pt.

# Material structure and photoelectric chemical characterizations

The crystal phase composition of the photocatalysts were characterized by X-ray powder diffractometry (XRD, Bruker D8 Advance). The surface microstructure and elemental mappings of the photocatalysts were measured by field emission scanning electron microscope (SEM, ZEISS Merlin, In-lens, Germany), transmission electron microscopy (TEM, JEM-2100F, Japan) and energy dispersive X-ray detector (EDX, Bruker, XFlash 5030T, Germany). The surface chemistry state was analyzed by X-ray photoelectron spectroscopy (XPS, Krato, Britain). The optical properties of the samples were

examined by ultraviolet—visible diffuse reflectance spectroscopy (DRS, U3010, Hitachi, Japan). The photoluminescence (PL) spectra of samples were tested by an F-7000 fluorescence spectrophotometer (Hitachi, Japan). The slit width of excitation and emission was 10 nm, the PMT voltage was 700 V, the excitation wavelength was 400 nm, and the scanning speed was 1200 nm min<sup>-1</sup>. The Surface photovoltaic (SPV) of samples were tested by surface photovoltage test system (CEL-SPS1000). The element content samples were analyzed by inductively coupled plasma atomic emission spectrometer (ICP-OES, Agilent 720 ES).

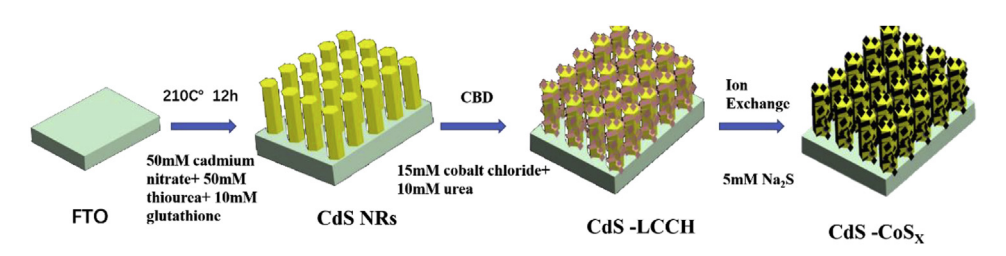
Photoelectrochemical performances of samples were performed using CHI660D electrochemical workstation with a three-electrode setup. Platinum net was used as the counter electrode, Ag/AgCl electrode was used as the reference electrode, and the as-prepared samples were served as the working electrode. The tests were conducted in electrolyte of 0.5 M Na<sub>2</sub>S-0.5 M Na<sub>2</sub>SO<sub>3</sub> mixed solution and light source was 300 W Xenon lamp with AM1.5 filter. Mott-Schottky plots acquired at 1000 Hz in 0.5 M Na<sub>2</sub>S-0.5 M Na<sub>2</sub>SO<sub>3</sub> mixed solution under dark condition.

#### Measurement of photocatalytic hydrogen production

The photocatalytic hydrogen evolution of the samples was carried out in a quartz closed photocatalytic hydrogen production system (CEL-SPH2N-D, Beijing). A piece of the structured catalyst (active area 3  $\times$  3 cm²) was immersed in 150 ml of a mixed solution containing 0.5 M Na<sub>2</sub>S-0.5 M Na<sub>2</sub>SO<sub>3</sub>. The photocatalytic reaction was conducted under visible light irradiation (300 W Xe lamp with 420 nm cut-off filter) and vacuum environment of less than -0.09 Mpa and temperature of 5 °C. Hydrogen was detected using GC-9790 gas chromatograph with molecular sieve 5 A packed column and thermal conductivity detector.

#### Measurement of photoelectrochemical hydrogen production

The photoelectrochemical reaction was implemented in CHI660D electrochemical workstation with three-electrode system. Platinum net was used as the counter electrode, Ag/ AgCl electrode was used as the reference electrode, the asprepared sample was served as the working electrode (effective area  $1\times 1.5~\text{cm}^2$ ). The hydrogen is collected by drainage as shown in Fig. S1. In the reaction system, the sacrificial agent is the mixed solution of 0.5M Na<sub>2</sub>S-0.5M Na<sub>2</sub>SO<sub>3</sub>. The simulated solar light source is 300 W Xenon lamp with light intensity of 82 mW cm<sup>-2</sup>, and the reaction temperature is room temperature (25 °C).



Scheme 1 - Preparation process of CdS-CoS<sub>x</sub>.

#### Results and discussion

#### Material structure characterizations

Fig. 1A shows that pure CdS is hexahedral prism structure, growing uprightly on FTO. Fig. 1(B–F) are SEM images of CdS NRs coated with  $CoS_x$ . It can be seen clearly that  $CoS_x$  nanosheets are uniformly distributed on the outer surface of CdS NRs, and the loading of  $CoS_x$  nanosheets gradually increases with the increase of deposition time. When the deposition time reaches 4 h, excess  $CoS_x$  completely covers the entire CdS NRs (Fig. 1F).

Fig. 2 shows TEM images of CdS-CoS $_x$ -3 and CdS. As shown in Fig. 2A, CdS exhibits short rod shape, the average length and average width of CdS have been measured to be 775 nm and 340 nm respectively. Fig. 2B is the HRTEM image of CdS, where the lattice diffraction fringes of the CdS (002) crystal plane can be observed. From Fig. 2C, it can be seen clearly that  $CoS_x$  nanosheets are layered on the surface of CdS. But it is hard to observe any lattice fringes of  $CoS_x$  in Fig. 2D, indicating that  $CoS_x$  exists mainly in amorphous form. The surface element distribution mappings of  $CoS_x$ -3 are shown in Fig. 2(E–G), corresponding to Cd, S, and Co, respectively, indicating that  $CoS_x$  nanosheets are uniformly distributed on the surface of the CdS NRs. The TEM images of other CdS- $CoS_x$  samples are shown in Fig. S2 (H-J).

The XPS spectra of CdS-CoS<sub>x</sub>-3 are shown in Fig. 3. In Fig. 3A, the characteristic peaks at 411.73 eV and 404.98 eV correspond to 3d<sub>3/2</sub> and 3d<sub>5/2</sub> of Cd<sup>2+</sup>, respectively. In Fig. 3B, the characteristic peaks at 162.50 eV and 161.30 eV are attributed to  $2p_{1/2}$  and  $2p_{3/2}$  of  $S^{2-}$ , respectively. The weak peak for elemental S can be found at around168.3 eV. Fig. 3C can be fitted to three pairs of peaks. One pair of the satellite peaks of Co are located on 803.38 eV and 787.04 eV. The other pair of peaks at 798.75 eV and 783.29 eV are assigned to 2p<sub>1/2</sub> and  $2p_{3/2}$  of  $Co^{3+}$ , and the third pair of peaks at 797.05 eV and 781.13eV are ascribed to  $2p_{1/2}$  and  $2p_{3/2}$  of  $Co^{2+}$ , respectively. According to the calculated peak areas, the content ratio of  $Co^{2+}$  to  $Co^{3+}$  is 1.76. Therefore, the prepared  $CoS_x$  is composed of Co<sup>2+</sup> and Co<sup>3+</sup>, mainly Co<sup>2+</sup>. Compared with the XPS spectra of CdS as shown in Fig. S3, it can be found that the peak positions of Cd and S in CdS-CoS<sub>x</sub>-3 have a little shift after

loading  $CoS_x$ , which is probably caused by the strong interaction between CdS and  $CoS_x$ . The XPS spectra for CdS-CoS<sub>x</sub>-3 sample before and after cycling stability test are shown in Fig. S4. It is obvious that the chemical state of CdS-CoS<sub>x</sub>-3 after stability test has hardly changed.

The XRD patterns of CdS-CoSx, CdS and CoSx powders are shown in Fig. 4A and Fig. S5. There is no significant difference between CdS and CdS-CoS<sub>x</sub>, and all samples have diffraction peaks corresponding to CdS and FTO, but no diffraction peaks of  $CoS_x$  are found in CdS-CoSx samples. The possible reason is that CoSx mainly exists in amorphous form, or the load of CoS<sub>x</sub> is too low. The XRD patterns of used CdS-CoS<sub>x</sub>-3 and CoS<sub>x</sub> powder are shown in Fig. S5. It obvious that the physical structure of CdS-CoS<sub>x</sub>-3 has hardly changed after stability test. The actual contents of Co, Cd, S elements in the CdS-CoS $_x$ -3 and CdS measured by inductively coupled plasma optical emission spectrometer (ICP-OES) are shown in Table S2. It is known that the real Co content of the prepared samples with optimum performance is 2.1%. Fig. 4B shows that the absorption intensity of the samples in the visible and ultraviolet light region increases with the extension of deposition time. When the deposition time extends to 4 h, the absorbance of CdS-CoS<sub>x</sub>-4 in the 300-500 nm region decreases, indicating that the excessive loading of CoS<sub>x</sub> is not conducive to the absorption of visible light. The curves of  $(Ah\nu)^2$  vs  $h\nu$  for all samples are shown in Fig. S6. It can be obtained that the band gap of CdS and CdS-CoS<sub>x</sub>-3 is 2.25 eV and 2.32 eV, respectively. Fig. 4C shows that the fluorescence intensity of CdS-CoS<sub>x</sub> is higher than that of CdS. This is because the carrier concentration of CdS-CoS<sub>x</sub> increases significantly after loading CoSx, leading to an increase in the amount of photogenerated carrier recombination. However, the fluorescence intensity of CdS-CoSx-3 is the lowest among all CdS-CoSx samples, indicating that proper CoS<sub>x</sub> loading can reduce the recombination of photogenerated carriers.

Fig. 5A and B show the time-resolved photoluminescence (TRPL) patterns of CdS and CdS-CoS<sub>x</sub>-3, respectively. TRPL spectra were fitted in polynomial R(t) =  $A_1 e^{(-t/\tau 1)} + A_2 e^{(-t/\tau 2)}$ . The fluorescent lifetime  $\tau_1$  and  $\tau_2$  were calculated to be 1.24 ns, 3.94 ns for CdS and 1.16 ns, 2.88 ns for CdS-CoS<sub>x</sub>-3, respectively. It is obvious that the fluorescence lifetime of CdS-CoS<sub>x</sub>-3 is slightly lower than that of CdS, which is possibly due to the

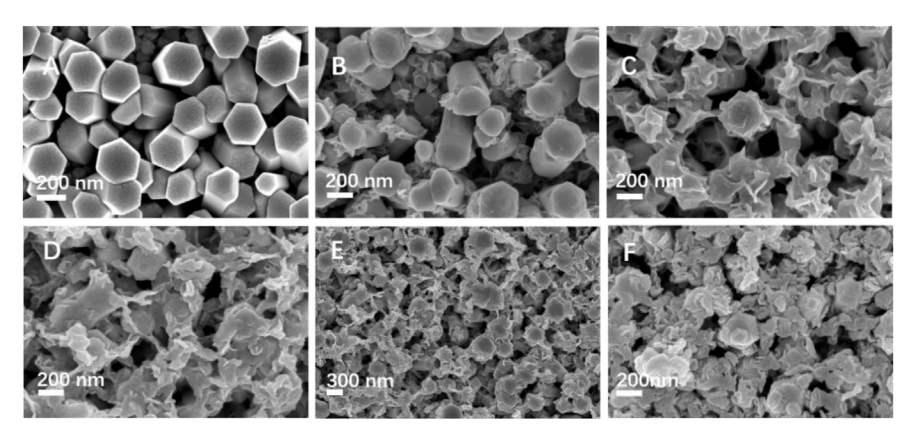


Fig. 1 – SEM images of (A) CdS, (B) CdS-CoS<sub>x</sub>-1, (C) CdS-CoS<sub>x</sub>-2, (D, E) CdS-CoS<sub>x</sub>-3, (F) CdS-CoS<sub>x</sub>-4.

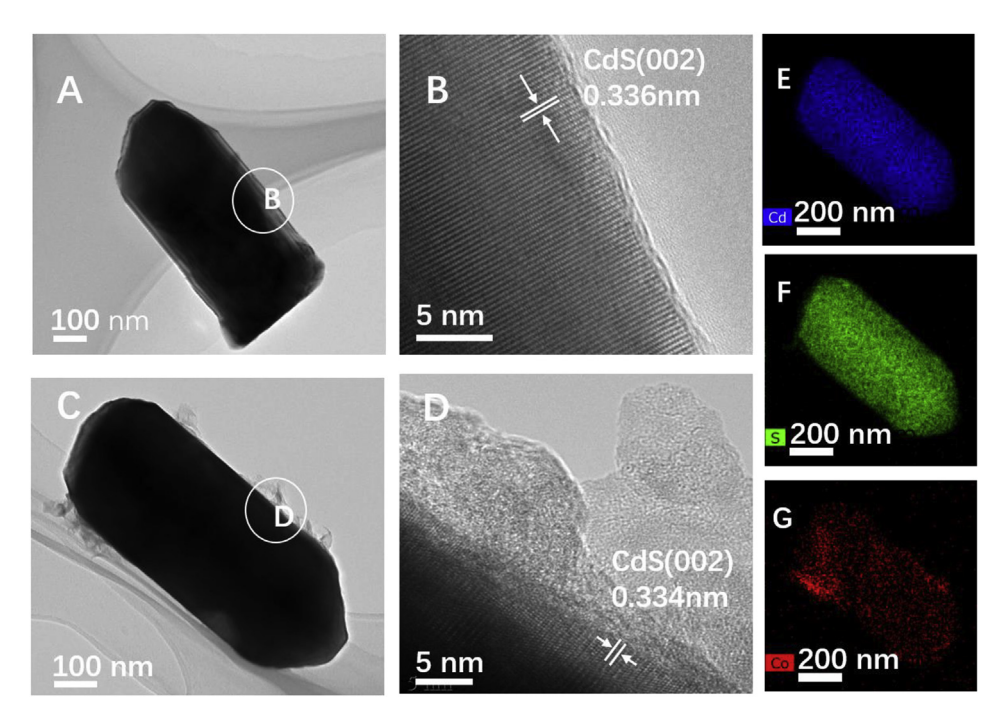


Fig. 2 - (A-B) TEM and HRTEM images of CdS. (C-D) TEM and HRTEM images of CdS-CoS $_x$ -3. (E-G) EDX element mappings of CdS-CoS $_x$ -3.

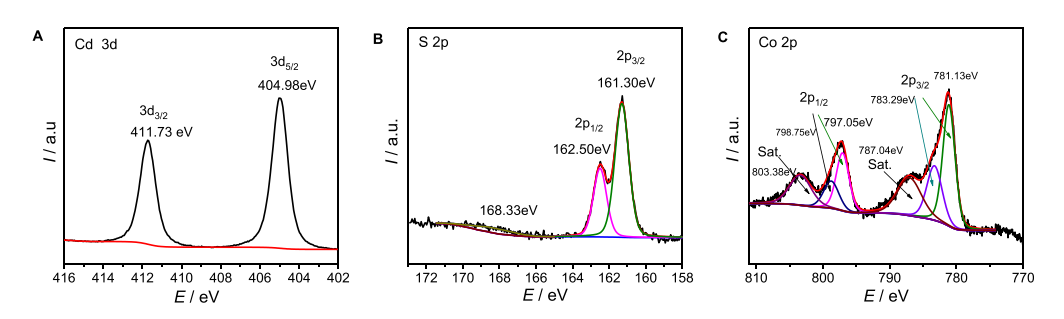


Fig. 3 – XPS spectra for (A) Cd 3d, (B) S 2p and (C) Co 2p of the CdS-CoS $_x$ -3.

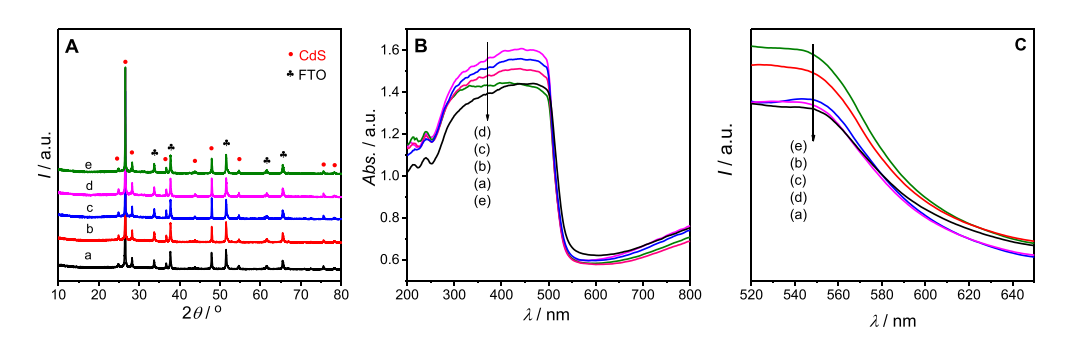


Fig. 4 – (A) XRD patterns, (B) UV–vis diffuse reflectance spectra and (C) photoluminescence patterns of (a) CdS, (b) CdS-CoS $_x$ -1, (c) CdS-CoS $_x$ -2, (d) CdS-CoS $_x$ -3, (e) CdS-CoS $_x$ -4.

increase of charge transfer rate of CdS after loading  $CoS_x$ . Fig. 5C exhibits the surface photovoltage (SPV) spectra of CdS and CdS- $CoS_x$ -3. It can be seen that the SPV value of CdS is higher than that of CdS- $CoS_x$ -3, indicating that less photogenerated electrons or more holes in CdS migrated to the

surface after loading  $CoS_x$ , and it is possibly because of the lower fermi level of  $CoS_x$  than that of CdS. As discussed above, we deem that an appropriate amount of  $CoS_x$  can effectively promote the transfer capability of photogenerated charge carrier in CdS.

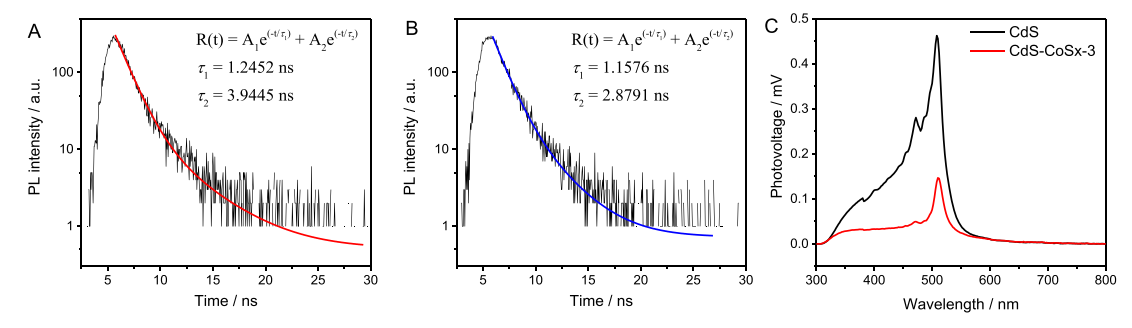


Fig. 5 – Time-resolved photoluminescence patterns of (A) CdS and (B) CdS-CoS $_x$ -3 and (C) surface photovoltaic patterns under the condition of completely protection from light of CdS and CdS-CoS $_x$ -3.

# Photocatalytic and photoelectrochemical hydrogen production

In order to study the carrier concentration and photocatalytic properties of all the samples, the Mott-Schottky curves and photocatalytic H<sub>2</sub> production were tested. Fig. 6A shows the slopes of normalized Mott-Schottky plots. As exhibited in Table S1, the calculated carrier concentration increases along with the increase of deposition time, but when the deposition time increases to 4 h, the excessive loading of CoSx reduces the carrier concentration. The calculated  $E_{CB}$  values of CdS and CdS-CoS<sub>x</sub>-3 are shown in Fig. S7. Combined with Fig. S6, it can be deduced that  $E_{VB}$  values of CdS and CdS-CoSx-3 are 3.33 eV and 3.35 eV, respectively. Under visible light irradiation, the hydrogen evolution rates of all samples are displayed in Fig. 6B. CdS without co-catalyst has almost no hydrogen produced by photocatalysis. After loading CoSx, the hydrogen production rate of CdS-CoS<sub>x</sub> increases rapidly, among which the hydrogen production rate of CdS-CoSx-3 is the highest (3.5  $\mu$ mol cm<sup>-2</sup> h<sup>-1</sup>). The cyclic stability of CdS-CoS<sub>x</sub>-3 for photocatalytic hydrogen production is displayed in Fig. 6C, demonstrating that the photocatalytic stability of CdS-CoS<sub>x</sub>-3 is very good after at least 5 cycles. However, the photocatalytic hydrogen production activity of CdS-CoS<sub>x</sub> is about 1/4 of that of CdS-Pt, indicating that the activity of CoS<sub>x</sub> as a co-catalyst is still lower than that of precious metal Pt (Fig. 6B-d and f).

The PEC hydrogen production was carried out with the schematic device shown in Fig. S1 and the results shown in Fig. 7A. It can be seen clearly from Fig. 7A that the PEC

hydrogen production rate of CdS-CoS $_{\rm x}$  samples is greatly improved compared with that of photocatalytic hydrogen production (Fig. 5B). The PEC hydrogen production rate of CdS-CoS $_{\rm x}$ -3 is 2.7 times that of CdS, reaching 168.6 µmol cm $^{-2}$  h $^{-1}$  (37.77 L m $^{-2}$  h $^{-1}$ ), which is the same as that of CdS–Pt. The recycling stability of CdS-CoS $_{\rm x}$ -3 for PEC hydrogen production is shown in Fig. 7B. After 5 cycles, the hydrogen production rate of the sample was reduced to 74%, indicating that the sample was subjected to some degree of photo-corrosion during PEC hydrogen production.

The linear sweep voltammetric (LSV) curves of all samples under dark and AM1.5 illumination are shown in Fig. 8A. At the positive bias voltage, all samples have much higher current densities under light irradiation than those in the dark, owing to the transfer of photogenerated electrons from the sample to counter electrode (Pt net). After deposited Pt on CdS, the photocurrent of CdS-Pt was obviously lower than that of pure CdS, which is possibly because of the excellent electron capture ability of the loaded Pt [35]. Fig. 8B shows the timepassed photocurrent curves (i-t curve) of the as-prepared samples at the bias voltage of 1.0 V (vs. RHE). It is obvious that the photocurrent density of CdS-Pt exhibits the smallest among all the samples. As the loading time of CoSx increases from 1 to 3 h, the photocurrent of CdS-CoSx decreases gradually. We deem that it is also because of the electron capture ability of the loaded CoS<sub>x</sub> as a reductive cocatalyst. While the loading time of CoSx reaches to 4 h, the photocurrent density of CdS- $CoS_x$  obviously increases. As shown in the SEM images (Fig. 1), the loaded CoS<sub>x</sub> obviously agglomerates in the CoS<sub>x</sub>-

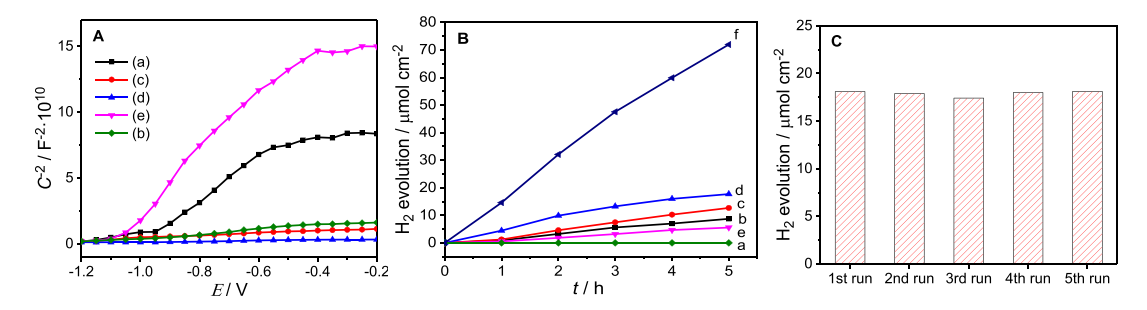


Fig. 6 – (A) Mott-Schottky plots acquired at 1000 Hz in 0.5 M Na<sub>2</sub>S-0.5 M Na<sub>2</sub>SO<sub>3</sub> mixed solution under dark condition. (B) The photocatalytic H<sub>2</sub> production in 0.5 M Na<sub>2</sub>S-0.5 M Na<sub>2</sub>SO<sub>3</sub> mixed solution under visible light irradiation on (a) CdS, (b) CdS-CoS<sub>x</sub>-1, (c) CdS-CoS<sub>x</sub>-2, (d) CdS-CoS<sub>x</sub>-3, (e) CdS-CoS<sub>x</sub>-4 and (f) CdS-Pt. (C) The recycling stability of CdS-CoS<sub>x</sub>-3 under visible light irradiation for 5 h.

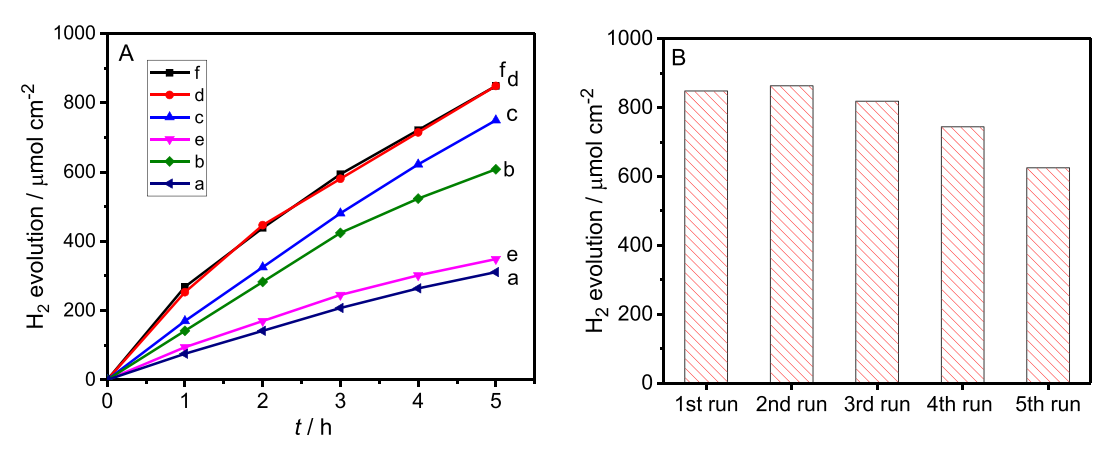


Fig. 7 — (A) The PEC hydrogen production at the potential of 0.6 V (vs. RHE) in 0.5 M Na<sub>2</sub>S-0.5 M Na<sub>2</sub>SO<sub>3</sub> solution under 300 W Xe lamp irradiation on (a) CdS, (b) CdS-CoS<sub>x</sub>-1, (c) CdS-CoS<sub>x</sub>-2, (d) CdS-CoS<sub>x</sub>-3, (e) CdS-CoS<sub>x</sub>-4, (f) CdS-Pt. (B) The recycling stability of CdS-CoS<sub>x</sub>-3 at the potential of 0.6 V (vs. RHE).

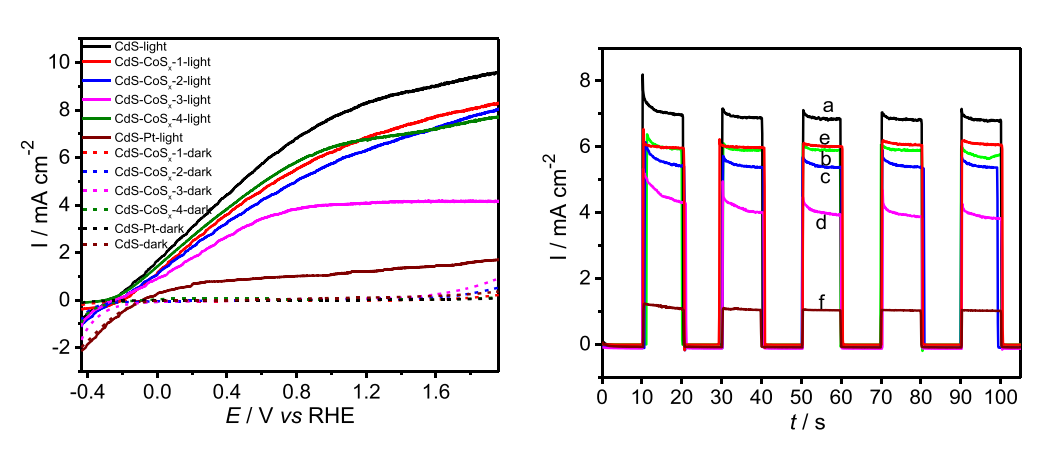


Fig. 8 – The polarization curves of samples (A), photocurrent density profiles under AM1.5 irradiation at the bias potential of 1.0 V ( $\nu$ s. RHE) (B) on (a) CdS, (b) CdS-CoS<sub>x</sub>-1, (c) CdS-CoS<sub>x</sub>-2, (d) CdS-CoS<sub>x</sub>-3, (e) CdS-CoS<sub>x</sub>-4 and (f) CdS-Pt.

CdS-4 sample. It is reported that the bulk  $CoS_x$  shows the properties of semiconductor [40]. According to the band structure of  $CoS_x$  and CdS, the electrons on the CB of  $CoS_x$  might transfer to the CB of CdS, hence increases the photocurrent density of CdS- $CoS_x$ .

# The reaction network analysis for photocatalytic hydrogen production

In the general PEC hydrogen production process, the photoelectrons of the working electrode are transferred to the counter electrode Pt by the external circuit to generate hydrogen. Therefore, the larger photocurrent corresponds to the higher photoelectrochemical hydrogen production rate. However, in this study, it is very interesting that the smaller photocurrent resulted in the higher photoelectrochemical hydrogen production rate. In fact, this phenomenon has also been found in TiO<sub>2</sub>/MoS<sub>2</sub> system [50].

In order to explain this abnormal result, a series of experiments (Fig. S8) were designed to explore the reaction process and the results were shown in Fig. 9. From Fig. 9A, it can be seen that in 0.5 M Na<sub>2</sub>S-0.5 M Na<sub>2</sub>SO<sub>3</sub> solution (Fig. S8A), Pt

alone produces little hydrogen. While CdS-CoS<sub>x</sub>-3 can produce hydrogen with the average hydrogen production rate of  $44~\mu mol~cm^{-2}~h^{-1}$  for 5 h. It should be noted that the photocatalytic hydrogen production rate of CdS-CoS<sub>x</sub>-3 in Fig. 9 is much higher than that in Fig. 5 because of different reaction temperatures and light sources. When Pt and CdS-CoS<sub>x</sub>-3 were simultaneously inserted into 0.5 M Na<sub>2</sub>S-0.5 M Na<sub>2</sub>SO<sub>3</sub> solution (Pt and CdS-CoS<sub>x</sub>-3 were not connected, Fig. S8B), the hydrogen production rate reaches 70  $\mu$ mol cm<sup>-2</sup> h<sup>-1</sup>, with 60% increase based on CdS-CoSx-3. For CdS alone, the average hydrogen production rate is 8  $\mu$ mol cm<sup>-2</sup> h<sup>-1</sup> for 5 h. However, the hydrogen production rate does not increase significantly when the Pt was inserted into solution. The hydrogen production performance of all samples was tested in the same case of Pt (Fig. S8B), and their hydrogen production rates are shown in Fig. S9. From these figures, all the photocatalysts exhibit enhanced hydrogen production rates when Pt is inserted simultaneously into the solution even if the Pt is not connected with the photocatalysts.

To this interesting phenomenon, we deduced the reason is that  $Na_2S_2O_3$  would be formed during the photocatalytic reaction in  $Na_2S-Na_2SO_3$  solution, then  $Na_2S_2O_3$  reacts with

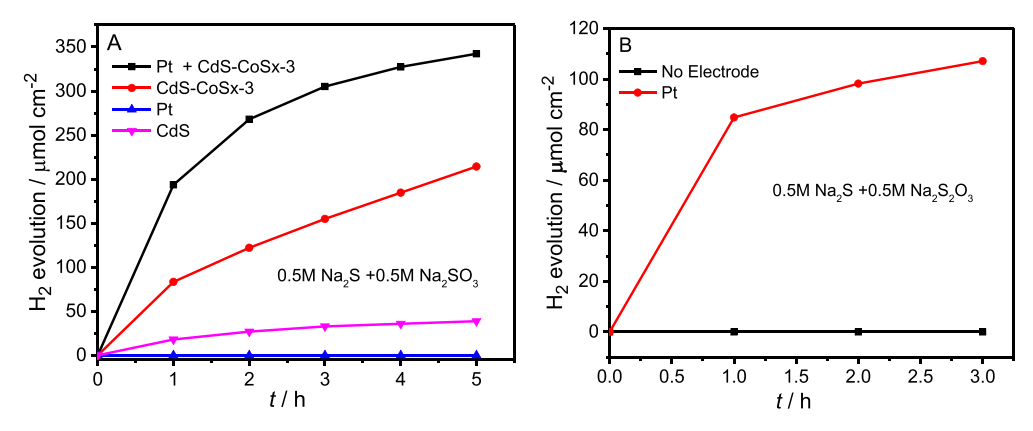


Fig. 9 – The photocatalytic  $H_2$  production rates in 0.5M  $Na_2S-0.5M$   $Na_2SO_3$  (A) and 0.5M  $Na_2S-0.5M$   $Na_2S_2O_3$  (B) solution under 300 W Xe lamp irradiation at different experimental situations (see Fig. S8).

water to release  $\rm H_2$  on the Pt electrode, thus increasing the hydrogen production rate. In order to verify our conjecture, Pt alone was inserted in 0.5M Na<sub>2</sub>S-0.5M Na<sub>2</sub>S<sub>2</sub>O<sub>3</sub> solution under irradiation for 3 h, as shown in Fig. S8A, large amounts of hydrogen were observed in this system. However,  $\rm H_2$  was not produced in the 0.5M Na<sub>2</sub>S-0.5M Na<sub>2</sub>S<sub>2</sub>O<sub>3</sub> solution under illumination without Pt, as shown in Fig. 9B. Therefore, it is preliminarily confirmed that Na<sub>2</sub>S<sub>2</sub>O<sub>3</sub> reacts with water to release  $\rm H_2$  on Pt electrode.

In order to further verify the formation of  $Na_2S_2O_3$ , we designed another experiment, as shown in Fig. S10. Firstly, a piece of  $CdS-CoS_x$ -3 alone was placed in 0.5M  $Na_2S-0.5M$   $Na_2SO_3$  solution under irradiation for 3 h, and then  $CdS-CoS_x$ -3 was taken out. Finally, Pt was put into the above solution and irradiated for 1 h. As expected, 1.2 mL hydrogen was produced, further indicating that the intermediate  $Na_2S_2O_3$  is formed in 0.5 M  $Na_2S-0.5$  M  $Na_2SO_3$  system.  $Na_2S_2O_3$  cannot be completely consumed in time on the  $CdS-CoS_x$  catalyst to generate hydrogen, while, Pt can enhance the redox reaction of  $Na_2S_2O_3$  with water to release  $H_2$ . Therefore, when Pt and  $CdS-CoS_x$  are both present in  $Na_2S-Na_2SO_3$  solution, the hydrogen production rate can be greatly improved.

Base on the above discussion, the photocatalytic reaction network in this catalytic system is proposed as follows (Eqs. (1)–(6)).

Photocatalytic reduction reaction:

$$2H_2O + 2e^- = H_2 + 2OH^- \tag{1}$$

 $E^0 = -0.828 \text{ V; } E = 0 \text{ us RHE}$ 

$$2SO_3^{2-} + 4e^- + 3H_2O = S_2O_3^{2-} + 6OH^-$$
 (2)

 $E^0 = -0.571V$  [51]; E = 0.257 vs RHE Photocatalytic oxidation reaction:

$$S^{2-} + 2h^{+} = S {3}$$

 $E^0 = -0.476 \text{ V } [51]; E = 0.354 \text{ us RHE}$ 

$$S + 6OH^- + 4h^+ = SO_3^{2-} + 3H_2O$$
 (4)

$$E^0 = -0.449 \text{ V } [51]; E = 0.369 \text{ us RHE}$$

$$SO_3^{2-} + 2h^+ + 2OH^- = SO_4^{2-} + H_2O$$
 (5)

 $E^0=-0.930~V$  [51]; E=-0.102~vs RHE Photochemical redox reaction (on Pt surface):

$$S_2O_3^{2-} + H_2O + 2OH^- = 2SO_3^{2-} + 2H_2$$
 (6)

In photocatalytic process, photogenerated electrons on CdS are transferred to CoSx to undergo a series of photocatalytic reduction reactions (Eqs. 1 and 2), and the holes left on CdS undergo photocatalytic oxidation reactions (Eqs. (3)-(5)), facilitating electron-hole separation and producing an intermediate species Na<sub>2</sub>S<sub>2</sub>O<sub>3</sub>. All reduction or oxidation potentials  $E^0$  in equations (1)–(5) represent the standard potentials in 1 M NaOH. These potentials were referenced to the reversible hydrogen electrode (RHE). In 0.5 M Na<sub>2</sub>S-0.5 M  $Na_2SO_3$  solution (pH = 13.6, close to the standard alkaline environment of 14), these reactions can occur theoretically on CdS-CoS<sub>x</sub> catalyst as shown in Fig. 10. According to the redox potentials, the reduction of Na<sub>2</sub>SO<sub>3</sub> into Na<sub>2</sub>S<sub>2</sub>O<sub>3</sub> is easier than H<sub>2</sub>O into H<sub>2</sub>. Furthermore, the aforementioned experimental results (Fig. 9B and Fig. S10) have verified that the intermediate Na<sub>2</sub>S<sub>2</sub>O<sub>3</sub> can occur photochemical redox reaction on Pt to release H<sub>2</sub> (Eq. (6)). Therefore, when Pt and CdS-CoS<sub>x</sub> are both present in system, the produced  $Na_2S_2O_3$  by photocatalysis on CdS-CoS<sub>x</sub> can diffuse to the Pt surface to generate H<sub>2</sub>, thus enhancing hydrogen production even though two electrodes are not connected (it can be understood that the external circuit photocurrent is 0).

Based on the reaction network analysis, it is easy to understand the abnormal phenomenon in PEC hydrogen production process, that is, low photocurrent leads to high hydrogen production rate. In PEC system, the external bias can promote the separation of the photogenerated electronhole, and the photoelectrons flow into counter electrode Pt (photocurrent) to reduce water to  $\rm H_2$ . Although pure CdS yield few  $\rm H_2$  in photocatalysis process due to recombination of electron-hole (Fig. 6B-a), the photogenerated electrons can reduce  $\rm H^+$  to  $\rm H_2$  on the Pt electrode when bias potential is

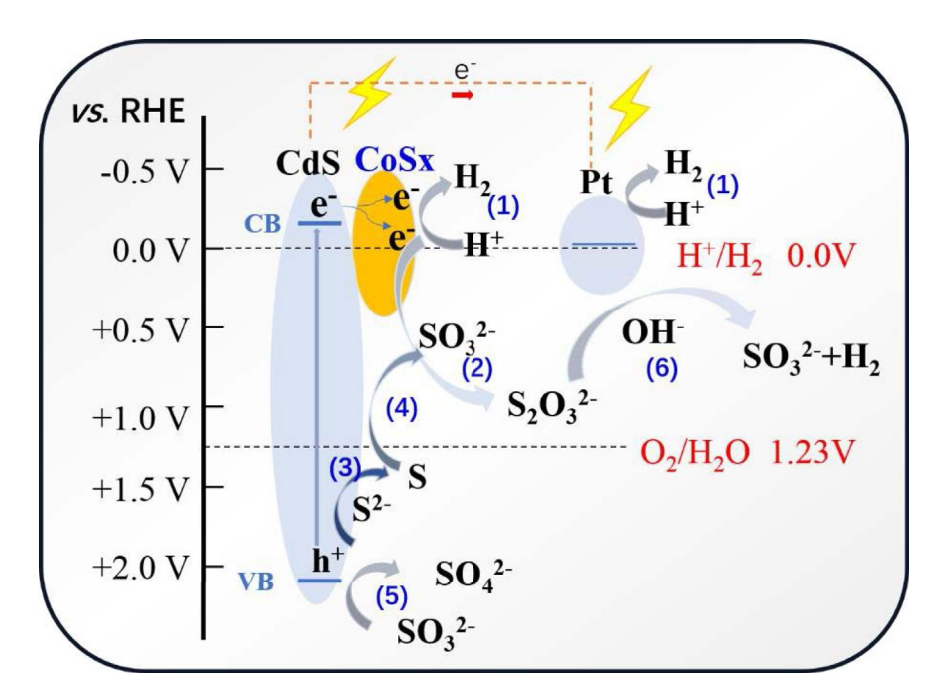


Fig. 10 - Reaction network of photocatalytic hydrogen production in Na<sub>2</sub>S-Na<sub>2</sub>SO<sub>3</sub> system.

applied, resulting in increased PEC hydrogen production (Fig. 7A-a). For the CdS-CoS<sub>x</sub> system, the photogenerated electrons on CdS are further separated under external bias and transferred to the co-catalyst CoSx firstly. The photocatalytic reduction reactions (Eqs.1 and 2) tend to occur on CoSx, and most photoelectrons are involved in these reactions, rather than flowing to the counter electrode through the external circuit, thus a decreased photocurrent. The easier the photocatalytic reaction (Eq. (2)) is, the smaller the photocurrent measured by the external circuit is, and the more  $S_2O_3^{2-}$  is generated, resulting in more  $H_2$  is generated on Pt electrode. Moreover, the rest of the photogenerated electrons also flows to the counter electrode (photocurrent) to participate in water reduction. It can be concluded that the stronger catalytic activity of CdS-CoSx is, the smaller photocurrent is and the higher hydrogen production efficiency is.

Through the above analysis, it is easy to explain that the photocatalytic hydrogen production activity of  $CdS-CoS_x$  (without Pt) is much lower than that of CdS-Pt (Fig. 6B-d and f). However, the PEC hydrogen production rate on  $CdS-CoS_x$  is obviously improved due to the synergistic effect with the Pt electrode and  $CdS-CoS_x$ . In particular, the  $CdS-CoS_x-3$  catalyst has the same PEC hydrogen production efficiency as CdS-Pt (Fig. 7B-d and f), indicating the potential of  $CoS_x$  replacing precious metal Pt in PEC hydrogen production.

# Conclusions

A novel structural catalyst  $CdS-CoS_x$  has been synthesized by a simple method, in which CoSx acts as co-catalyst to accept photoexcited electrons of CdS, thereby improving the hydrogen production activity and stability of CdS. Under the simulated solar light, the PEC hydrogen production rate using

CdS-CoS $_{\rm x}$  as photoanode reaches 168.6 µmol cm $^{-2}$  h $^{-1}$  (37.77 L m $^{-2}$  h $^{-1}$ ), which is 2.7 times that of CdS and the same as that of CdS–Pt. The prepared CdS-CoS $_{\rm x}$  is easy to recycle, and CoS $_{\rm x}$  shows the potential of replacing precious metal Pt. More important, in this work, an abnormal relationship between photocurrent and hydrogen production was found in the Na $_{\rm 2}$ S–Na $_{\rm 2}$ SO $_{\rm 3}$  system for PEC hydrogen production. A series of experiments were reasonably designed to explain this abnormal phenomenon and reveal the photocatalytic and PEC hydrogen production characteristics. The reaction network in Na $_{\rm 2}$ S–Na $_{\rm 2}$ SO $_{\rm 3}$  system for photocatalytic hydrogen production has been proposed and verified for the first time. It can be concluded that the stronger catalytic activity of CdS-CoS $_{\rm x}$  is, the smaller photocurrent is and the higher hydrogen production efficiency is.

### Acknowledgements

We acknowledge the financial support from the National Natural Science Foundation of China (No. 21673080, 51706231).

# Appendix A. Supplementary data

Supplementary data to this article can be found online at https://doi.org/10.1016/j.ijhydene.2019.09.078.

REFERENCES

[1] Zou X, Zhang Y. Noble metal-free hydrogen evolution catalysts for water splitting. Chem Soc Rev 2015;44:5148–80.

- [2] He H, Cao J, Guo M, Lin H, Zhang J, Chen Y, Chen S. Distinctive ternary CdS/Ni<sub>2</sub>P/g-C<sub>3</sub>N<sub>4</sub> composite for overall water splitting: Ni<sub>2</sub>P accelerating separation of photocarriers. Appl Catal B Environ 2019;249:246–56.
- [3] Hu J, Zhang S, Cao Y, Wang H, Yu H, Peng F. Novel highly active anatase/rutile TiO<sub>2</sub> photocatalyst with hydrogenated heterophase interface structures for photoelectrochemical water splitting into hydrogen. ACS Sustainable Chem Eng 2018;6:10823-32.
- [4] Liu X, Iocozzia J, Wang Y, Cui X, Chen Y, Zhao S, Li Z, Lin Z. Noble metal-metal oxide nanohybrids with tailored nanostructures for efficient solar energy conversion, photocatalysis and environmental remediation. Energy Environ Sci 2017;10:402–34.
- [5] Low J, Yu J, Jaroniec M, Wageh S, Al-Ghamdi AA. Heterojunction photocatalysts. Adv Mater 2017;29:1601694.
- [6] Zhong D, Liu W, Tan P, Zhu A, Liu Y, Xiong X, Pan J. Insights into the synergy effect of anisotropic {001} and {230} facets of BaTiO<sub>3</sub> nanocubes sensitized with CdSe quantum dots for photocatalytic water reduction. Appl Catal B Environ 2018;227:1–12.
- [7] Xiao M, Luo B, Wang SC, Wang LZ. Solar energy conversion on g-G<sub>3</sub>N<sub>4</sub> photocatalyst: light harvesting, charge separation, and surface kinetics. J Energy Chem 2018;27:1111–23.
- [8] Vu M-H, Sakar M, Nguyen Chinh-Chien. Trong-On. Do, Chemically bonded Ni cocatalyst onto the S doped g-C<sub>3</sub>N<sub>4</sub> nanosheets and their synergistic enhancement in H<sub>2</sub> production under sunlight irradiation. ACS Sustainable Chem Eng 2018;6:4194–203.
- [9] Wang ZJ, Liu Z, Chen JZ, Yang HB, Luo JQ, Gao JJ, Zhang JM, Yang CJ, Jia SP, Liu B. Self-assembly of three-dimensional CdS nanosphere/graphene networks for efficient photocatalytic hydrogen evolution. J Energy Chem 2019;31:34—8.
- [10] Reddy DA, Kim EH, Gopannagari M, Kim Y, Kumar DP, Kim TK. Few layered black phosphorus/MoS<sub>2</sub> nanohybrid: a promising co-catalyst for solar driven hydrogen evolution. Appl Catal B Environ 2019;241:491–8.
- [11] Reddy DA, Park H, Ma R, Kumar DP, Lim M, Kim TK. Heterostructured WS<sub>2</sub>-MoS<sub>2</sub> ultrathin nanosheets integrated on CdS nanorods to promote charge separation and migration and improve solar-driven photocatalytic hydrogen evolution. ChemSusChem 2017;10:1563-70.
- [12] Cao S, Yan X, Kang Z, Liang Q, Liao X, Zhang Y. Band alignment engineering for improved performance and stability of ZnFe<sub>2</sub>O<sub>4</sub> modified CdS/ZnO nanostructured photoanode for PEC water splitting. Nano Energy 2016;24:25—31.
- [13] Zhang J, Li W, Li Y, Zhong L, Xu C. Self-optimizing bifunctional CdS/Cu<sub>2</sub>S with coexistence of light-reduced CuO for highly efficient photocatalytic  $H_2$  generation under visible-light irradiation. Appl Catal B Environ 2017;217:30–6.
- [14] Iqbal S, Pan Z, Zhou K. Enhanced photocatalytic hydrogen evolution from in situ formation of few-layered MoS<sub>2</sub>/CdS nanosheet-based van der Waals heterostructures. Nanoscale 2017;9:6638–42.
- [15] Xu Z, Yan H, Wu G, Ma G, Wen F, Lu W, Li C. Enhancement of photocatalytic H<sub>2</sub> evolution on CdS by loading MoS<sub>2</sub> as cocatalyst under visible light irradiation. J Am Chem Soc 2008;130:7176-7.
- [16] Wong AB, Brittman S, Yu Y, Dasgupta NP, Yang P. Core-shell  $CdS-Cu_2S$  nanorod array solar cells. Nano Lett 2015;15:4096-101.
- [17] Reddy DA, Kim HK, Kim Y, Lee S, Choi J, Islam MJ, Kumar DP, Kim TK. Multicomponent transition metal phosphides derived from layered double hydroxide double-shelled nanocages as an efficient non-precious co-catalyst for hydrogen production. J Mater Chem 2016;4:13890—8.

- [18] Xing Z, Zhang J, Cui J, Yin J, Zhao T, Kuang J, Xiu Z, Wan N, Zhou W. Recent advances in floating TiO<sub>2</sub>-based photocatalysts for environmental application. Appl Catal B Environ 2018;225:452–67.
- [19] Ai G, Li H, Liu S, Mo R, Zhong J. Solar water splitting by TiO<sub>2</sub>/CdS/Co-Pi nanowire array photoanode enhanced with Co-Pi as hole transfer relay and CdS as light absorber. Adv Funct Mater 2015;25:5706–13.
- [20] Wakerley DW, Kuehnel MF, Orchard KL, Ly KH, Rosser TE, Reisner E. Solar-driven reforming of lignocellulose to H<sub>2</sub> with a CdS/CdOx photocatalyst. Nat Energy 2017;2:17021.
- [21] Ma D, Shi J-W, Zou Y, Fan Z, Ji X, Niu C, Wang L. Rational design of CdS@ZnO core-shell structure via atomic layer deposition for drastically enhanced photocatalytic H<sub>2</sub> evolution with excellent photostability. Nano Energy 2017;39:183–91.
- [22] Li H, Wang X, Xu J, Zhang Q, Bando Y, Golberg D, Ma Y, Zhai T. One-dimensional CdS nanostructures: a promising candidate for optoelectronics. Adv Mater 2013;25:3017–37.
- [23] Li Q, Li X, Wageh S, Al-Ghamdi AA, Yu J. CdS/graphene nanocomposite photocatalysts. Adv Energy Mater 2015;5:1500010.
- [24] Jiang D, Sun Z, Jia H, Lu D, Du P. A cocatalyst-free CdS nanorod/ZnS nanoparticle composite for high-performance visible-light-driven hydrogen production from water. J Mater Chem 2016;4:675–83.
- [25] Dai K, Lv J, Zhang J, Zhu G, Geng L, Liang C. Efficient visible-light-driven splitting of water into hydrogen over surface-fluorinated anatase TiO<sub>2</sub> nanosheets with exposed {001} facets/layered CdS-diethylenetriamine nanobelts. ACS Sustainable Chem Eng 2018;6:12817–26.
- [26] Reddy DA, Choi J, Lee S, Kim Y, Hong S, Kumar DP, Kim TK. Hierarchical dandelion-flower-like cobalt-phosphide modified CdS/reduced graphene oxide-MoS<sub>2</sub> nanocomposites as a noble-metal-free catalyst for efficient hydrogen evolution from water. Catal Sci Technol 2016;6:6197–206.
- [27] Wang H, Jin Z, Hao X. CoSe<sub>2</sub>/CdS-diethylenetriamine coupled with P clusters for efficient photocatalytic hydrogen evolution. Dalton Trans 2019;48:4015–25.
- [28] Liu Y, Yang S, Zhang S, Wang H, Yu H, Cao Y, Peng F. Design of cocatalyst loading position for photocatalytic water splitting into hydrogen in electrolyte solutions. Int J Hydrogen Energy 2018;43:5551–60.
- [29] Reddy DA, Park H, Hong S, Kumar DP, Kim TK. Hydrazineassisted formation of ultrathin MoS<sub>2</sub> nanosheets for enhancing their co-catalytic activity in photocatalytic hydrogen evolution. J Mater Chem 2017;5:6981–91.
- [30] Yang H, Jin Z, Wang G, Liu D, Fan K. Light-assisted synthesis MoSx as a noble metal free cocatalyst formed heterojunction CdS/Co<sub>3</sub>O<sub>4</sub> photocatalyst for visible light harvesting and spatial charge separation. Dalton Trans 2018;47:6973–85.
- [31] Liang W, Chen Y, Lin Y, Wu H, Yuan R, Li Z. MoS<sub>2</sub> as non-noble-metal co-catalyst for photocatalytic hydrogen evolution over hexagonal ZnIn<sub>2</sub>S<sub>4</sub> under visible light irradiations. Appl Catal B Environ 2014;144:521–7.
- [32] Liu X, Liang X, Wang P, Huang B, Qin X, Zhang X, Dai Y. Highly efficient and noble metal-free NiS modified Mn<sub>x</sub>Cd<sub>1-x</sub>S solid solutions with enhanced photocatalytic activity for hydrogen evolution under visible light irradiation. Appl Catal B Environ 2017;203:282–8.
- [33] Fang X, Song J, Pu T, Wang C, Yin C, Wang J, Kang S, Shi H, Zuo Y, Wang Y, Cui L. Graphitic carbon nitride-stabilized CdS@CoS nanorods: an efficient visible-light-driven photocatalyst for hydrogen evolution with enhanced photocorrosion resistance. Int J Hydrogen Energy 2017;42:28183–92.

- [34] Lang D, Cheng F, Xiang Q. Enhancement of photocatalytic H<sub>2</sub> production activity of CdS nanorods by cobalt-based cocatalyst modification. Catal Sci & Technol 2016;6:6207-16.
- [35] Lin Y, Liu Y, Li Y, Cao Y, Huang J, Wang H, Yu H, Liang H, Peng F. Dual functional  $CuO_{1-x}$  clusters for enhanced photocatalytic activity and stability of a Pt cocatalyst in an overall water-splitting reaction. ACS Sustainable Chem Eng 2018;6:17340–51.
- [36] Lin Y, Yang S, Liu Y, Zhang S, Wang H, Yu H, Peng F. In-situ photo-deposition  $CuO_{1-x}$  cluster on  $TiO_2$  for enhanced photocatalytic  $H_2$  production activity. Int J Hydrogen Energy 2017;42:19942–50.
- [37] Zhang L, Jin Z, Ma X, Zhang Y, Wang H. Properties of iron vanadate over CdS nanorods for efficient photocatalytic hydrogen production. New J Chem 2019;43:3609–18.
- [38] Yang H, Jin Z, Liu D, Fan K, Wang G. Visible light harvesting and spatial charge separation over the creative Ni/CdS/Co<sub>3</sub>O<sub>4</sub> photocatalyst. J Phys Chem C 2018;122:10430–41.
- [39] Zhang F, Zhuang H-Q, Song J, Men Y-L, Pan Y-X, Yu S-H. Coupling cobalt sulfide nanosheets with cadmium sulfide nanoparticles for highly efficient visible-light-driven photocatalysis. Appl Catal B Environ 2018;226:103—10.
- [40] Qiu B, Zhu Q, Du M, Fan L, Xing M, Zhang J. Efficient solar light harvesting CdS/Co9 S8 hollow cubes for Z-scheme photocatalytic water splitting. Angew Chem Int Ed 2017;56:2684—8.
- [41] Zheng M, Ding Y, Yu L, Du X, Zhao Y. In Situ grown pristine cobalt sulfide as bifunctional photocatalyst for hydrogen and oxygen evolution. Adv Funct Mater 2017;27:1605846.
- [42] Yu Z, Meng J, Xiao J, Li Y, Li Y. Cobalt sulfide quantum dots modified TiO<sub>2</sub> nanoparticles for efficient photocatalytic hydrogen evolution. Int J Hydrogen Energy 2014;39:15387–93.
- [43] Lin C-Y, Mersch D, Jefferson DA, Reisner E. Cobalt sulphide microtube array as cathode in photoelectrochemical water splitting with photoanodes. Chem Sci 2014;5:4906–13.

- [44] Kung CW, Chen HW, Lin CY, Huang KC, Vittal R, Ho KC. CoS acicular nanorod arrays for the counter electrode of an efficient dye-sensitized solar cell. ACS Nano 2012;6:7016–25.
- [45] Reddy DA, Park H, Gopannagari M, Kim EH, Lee S, Kumar DP, Kim TK. Designing CdS mesoporous networks on MOF derived Co-C@Co9S8 double-shelled nanocages as a redox-mediator-free Z-scheme photocatalyst with superior photocatalytic efficiency. ChemSusChem 2017;11:245–53.
- [46] Wang S, Guan BY, Wang X, Lou XWD. Formation of hierarchical  $\text{Co}_9\text{S}_8$ @Zn $\text{In}_2\text{S}_4$  heterostructured cages as an efficient photocatalyst for hydrogen evolution. J Am Chem Soc 2018;140:15145–8.
- [47] Liu R, Sun Z, Song X, Zhang Y, Xu L, Xi L. Toward non-precious nanocomposite photocatalyst: an efficient ternary photoanode TiO<sub>2</sub> nanotube/Co<sub>9</sub>S<sub>8</sub>/polyoxometalate for photoelectrochemical water splitting. Appl Catal A-Gen 2017;544:137–44.
- [48] Wang B, Peng F, Yang S, Cao Y, Wang H, Yu H, Zhang S. Hydrogenated CdS nanorods arrays/FTO film: a highly stable photocatalyst for photocatalytic H<sub>2</sub> production. Int J Hydrogen Energy 2018;43:17696–707.
- [49] Yuan Z, Tang R, Zhang Y, Yin L. Enhanced photovoltaic performance of dye-sensitized solar cells based on  $Co_9S_8$  nanotube array counter electrode and  $TiO_2/g-C_3N_4$  heterostructure nanosheet photoanode. J Alloy Comp 2017;691:983–91.
- [50] Liu Y, Li Y, Peng F, Lin Y, Yang S, Zhang S, Wang H, Cao Y, Yu H. 2H- and 1T- mixed phase few-layer MoS<sub>2</sub> as a superior to Pt co-catalyst coated on TiO<sub>2</sub> nanorod arrays for photocatalytic hydrogen evolution. Appl Catal B Environ 2019;241:236–45.
- [51] Weast RC, Astle MJ, Beyer WH. CRC handbook of chemistry and physics. Boca Raton, FL: CRC press; 1988.